Received: 5 February 2021 | Revised: 26 March 2021 | Accepted: 29 March 2021

DOI: 10.1002/app.50881

ARTICLE

Journal of Applied Polymer Science WILEY

Structural silicone sealants after exposure to laboratory test for durability assessment

Wilma Wallau[1] | **Christoph Recknagel**[1] | **Glen J. Smales**[2]

[1]7.1 Building Materials, Bundesanstalt für Materialforschung und –prüfung, Berlin, Germany

[2]6.5 Synthesis and Scattering of Nanostructured Materials, Bundesanstalt für Materialforschung und –prüfung, Berlin, Germany

Correspondence
Wilma Wallau, 7.1 Building Materials, Bundesanstalt für Materialforschung und –prüfung, Unter den Eichen 87, 12205 Berlin, Germany.
Email: wilma.wallau@bam.de

Funding information
This work was partly supported by the German Federal Ministry of Economy and Technology under the grant, Grant/Award Number: MNPQ 22/10

Abstract

During the service life of structural sealant glazing (SSG) facades, the load-bearing capacity of the silicone bonds needs to be guaranteed. Laboratory tests can assess the durability of SSG-systems based on mechanical characteristics of the bond after simultaneous exposure to both climatic and mechanical loads. This article studies how the material characteristics of two common structural sealants are affected by laboratory and field exposure. Dynamic mechanical analysis (DMA) confirms a reduction in the dynamic modulus of exposed silicone samples. Results from thermogravimetric analysis, Fourier-transform infrared spectroscopy, differential scanning calorimetry, and small-angle X-ray scattering/wide-angle X-ray scattering show differences between the two sealants and indicate no/minor changes in the composition and morphology of the laboratory and field exposed sealants. Mechanical characterization methods, such as DMA, and tensile and shear testing of the structural bond, are shown to be sensitive toward the combined climatic and mechanical loadings, and are hence suitable for studying degradation mechanisms of structural sealants.

KEYWORDS

aging, analytical methods, fatigue, silicone elastomer, structural sealant glazing

1 | INTRODUCTION

In structural sealant glazing (SSG) systems, the adhesive bonds between glass panes, and the predominantly metal substructures, are formed by silicones. Compared to polyurethane and epoxy adhesives, silicones exhibit low strength and stiffness making them particularly suitable for the absorption of movement.[1] Joint dimensions are designed so that there is sufficient strength for the structural bond, through increasing the bonding area, while the flexibility is resultant from having a large bonding thickness (above 6 mm).[2]

Compared to alternative glass facade solutions, SSG-systems avoid the accumulation of local stress in the glass pane, and thermal bridging when retaining devices are omitted. In these cases, long-time serviceability of the structural bond is necessary as bond failure, and the dropping of facade elements, can cause fatal accidents. Although SSG-bonds are simultaneously exposed to climatic, mechanical, and chemical loads, which are believed to interact during aging and fatigue mechanisms, current regulations

[Corrections added on 19 May 2021, after first online publication: The degree symbol for 'C' unit has been amended in the text.]

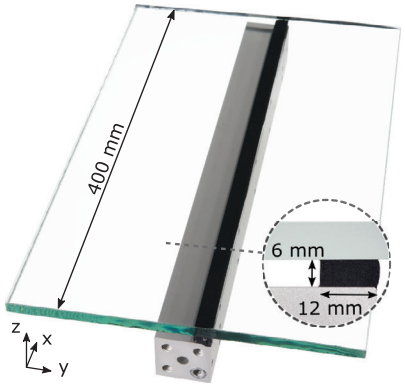

FIGURE 1 System specimen: structural bond between glass pane and aluminum frame resembling common SSG-joint designs. SSG, structural sealant glazing [Color figure can be viewed at wileyonlinelibrary.com]

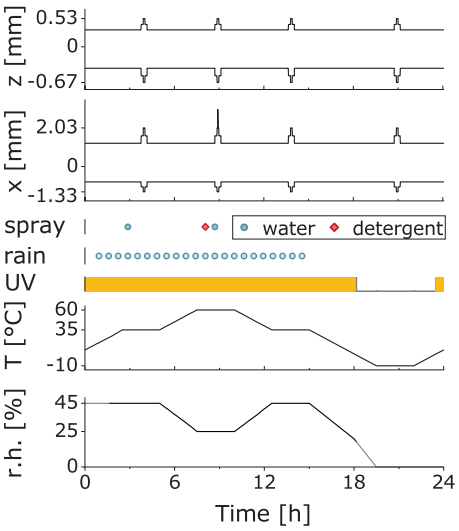

FIGURE 2 One load cycle of the durability test program: Amplitudes of 2526 sinusoidal displacement cycles in x- and z-direction and the simultaneously applied climatic loading with temperature, humidity, and UV-radiation control, application of spray onto the sealant bead, and rain events [Color figure can be viewed at wileyonlinelibrary.com]

comprise durability tests that disassociate these testing protocols. ETAG 002, for instance, regulates fatigue cycling and accelerated weathering in separate testing programs.[2]

In this context, a durability testing method was developed at BAM (Bundesanstalt für Materialforschung und -prüfung), that experimentally simulates the exposure of a common SSG-joint during a 50-year service life. The test subjects system specimens (Figure 1) to 50 consecutive load cycles (Figure 2) that apply both mechanical and climatic loading simultaneously. During these combined loadings, stress–strain data is continuously recorded to evaluate the dynamic mechanical behavior of the specimens for performance assessment under varying exposure conditions. After exposure, mechanical characteristics of the structural bond are obtained, for example, from tensile and shear tests of cut-out sections of the specimens. Previously, we have explained such a testing methodology[3] and applied it to two structural sealants.[4] The combined laboratory exposure caused a notable decrease in the mechanical properties of the structural bonds, namely the tensile and shear strengths, moduli and yield strain. It further showed, that cyclic weathering of specimens alone had no such effect on the mechanical characteristics.[4]

This article looks at how the divergence of mechanical characteristics, for joint specimens under different exposure conditions, relates to changes in the composition and/or morphology of the structural silicone. Characterization methods are applied to assess how the structural silicone materials are affected by the combined loading during a durability test, by cyclic weathering, and by exposure in the field.

This is done in the hope that the application of sensitive characterization methods can aid in forming a better understanding of aging and fatigue mechanisms of structural silicones. By comparing effects of both laboratory and real exposures, the suggested durability test methodology could be validated and advanced. Such characterization method could also be applied to structural health monitoring of SSG-systems in service for assessing the degree of degradation or the remaining service life.

1.1 | Silicone rubber

Due to their hybrid organic/inorganic molecular structures, silicone rubbers combine unusual characteristics, such as high-temperature stability and flexibility at low temperatures.[5] The cross-linked and entangled polydimethylsiloxane (PDMS) chains gain their mechanical strength and stiffness from reinforcing fillers.[6] Common reinforcing and semi-reinforcing fillers, such as carbon black, silica, and calcium carbonate are mostly aggregated nanoparticles, which can again form even larger agglomerates when dispersed in the rubber matrix.[7] This network of filler aggregates and the physical bonds formed between their surface and the silicone chains (bound rubber) in-turn decreases the mobility of the PDMS chains.[8] Moreover, silicone shows excellent adhesion on common substrates of SSG-bonds[9] like glass and anodised aluminum.

Commercially available structural silicone products are complex composites, with their compositions and manufacturing details often unknown to researchers, complicating comprehensive analysis and the

understanding of aging/fatigue mechanisms.[10] Nonetheless, it is possible to deploy a multitude of different characterization methods to obtain some information on the composition, morphology and relevant characteristics. Dynamic mechanical analysis (DMA) is a widespread method to characterize the complex mechanical behavior of elastomers, with its elastic and viscous component. Over a range of frequencies or temperatures, two dynamic mechanical characteristics, e.g. the storage modulus and loss factor, suffice to identify phase transitions, such as crystallization, melting of crystalline phases and glass transition. While rubber components commonly operate at temperatures associated with the rubbery plateau, which describes the range between glass transition and melting, the melting temperature of silicones of about −40°C is below common operation temperatures. Glass transition of silicones, which occurs at very low temperatures below −120°C, is not affected by fillers.[11,12] These characteristic temperatures or temperature ranges can also be determined applying differential scanning calorimetry (DSC), that further yields the enthalpy of phase transitions. The melting enthalpy relates to the degree of crystallinity, that correlates to the PDMS chain length.[13] The crosslinking density of elastomers can be estimated from the modulus of elasticity or from solvent swelling.[14]

The concentration, particle size, and dispersion of many fillers are known to influence not only mechanical, but also other characteristics of silicone rubber. For example, dielectric silicones with increased concentrations of carbon black have higher electric permittivity and elastic moduli.[15] It has also been shown that the increased surface of smaller calcium carbonate particles can enhance the filler network and thus the dynamic mechanical moduli of the composite.[16,17] Moreover, particle size distributions of fillers were found to be affected by the incorporation to elastomers,[7,18] that is, small-angle X-ray scattering (SAXS) measurements of carbon black fillers have shown a shift toward larger diameters when mixed with natural rubber whereas the size of calcium carbonate aggregates were observed to reduce after mixing with silicone rubber.

1.2 | Aging

Adhesive and cohesive mechanical characteristics of the structural bond must sustain throughout the service life of an SSG-joint. Accordingly, tensile and shear tests are commonly conducted to evaluate the performance and assess the effects of artificial aging[19–21] or natural exposure.[22,23] Depending on the type of silicone and exposure procedure, the strength and moduli are found to both decrease[13,24] and increase[25,26] in the literature. Aging of silicones can thus cause both, the formation of new crosslinks, and chain scission at existing crosslinks.[25,27]

The applicability of a wide range of characterization methods to study aging of sealants was reviewed by Wolf and Oba.[10] Thermogravimetric analysis (TGA) of a black one-component silicone exposed to water and UV-radiation indicated strong weatherability of the sealant.[28] Despite a significant reduction of the tensile strength of silicone rubber due to accelerated aging (6-week immersion in industrial lubricant at 195°C), Fourier-transform infrared spectra (FTIR) showed no changes of the surface chemistry.[24]

1.3 | Fatigue

Studies on the fatigue behavior of structural silicones[29–31] expediently focus on performance-indicating mechanical characteristics like tensile and shear moduli and strength. To the best of our knowledge, the possible effects of mechanical loading of SSG silicones has not been studied beyond their mechanical characteristics. Instead, studies on the fatigue of silicones used in electrical applications, which can also be exposed to cyclic mechanical loading, are more commonly deployed with analytical characterization methods such as DSC, FTIR, TGA.[26,32]

2 | EXPERIMENTAL

The durability test program includes the simultaneous exposure of two system specimens (Figure 1) to combined loading. In addition, a third specimen is exposed to the climatic load function only, and a fourth remains non-exposed for reference. The system specimens studied in this article stem from the same durability test series presented previously.[3,4] After exposure, all four specimens were water jet cut into sections to gain samples for characterization of the bond and sealant material, as shown in Figure 3. The silicone bead of the 37 mm-section was carefully separated from the adherends with a utility knife. A splitter was then applied to obtain two samples (each 35 x 3 x 12 mm^3) for DMA. From the remaining 2 mm-sections, small-sized samples were taken from positions at the weathered surface for DSC, TGA, and FTIR. The samples previously subjected to DMA were microtomed to approximate 100 μm-samples for SAXS/wide-angle X-ray scattering (WAXS) measurements.

2.1 | SSG silicones

The durability tests were conducted in two series (A and B) with two different SSG silicones (*a* and *b*), which formed the structural bond of the system specimens.

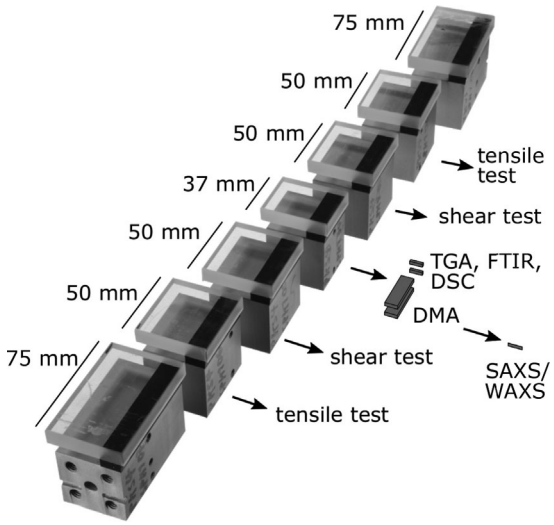

FIGURE 3 Water-jet cut samples from the system specimen for bond and material characterization

Additionally, samples from real SSG-joints of the same two types of structural silicone were characterized. These joints had been in-service for about 13 years (sealant *a*) and at least 23 years (sealant *b*).

The applied structural silicones are commercial products and their specific formulations are unknown to the authors. However, some information are available in the literature.[33] Both structural sealants are neutral addition-curing from two components: a viscous base component and a liquid or viscous curing agent. The components are mixed at a ratio of about 10:1 to a workable black paste that cures at room temperature. The white base component contains vinyl-endblocked PDMS, which constitute the non-cross-linked polymer chains with their siloxane backbone. The black curing agent contains the cross-linker, cyclic or linear silicon hydrides. Additional ingredients include a catalyst, most commonly a platinum compound, an inhibitor to prolong workability, an adhesion promoter, and fillers.

2.2 | Tensile and shear tests

As specified in ETAG 002, tensile and shear tests with small-scale specimens are employed here for assessing mechanical characteristics of the bond. Accordingly, the 50 mm-sections, shown in Figure 3, were subjected to tensile or shear tests at constant strain rate 5 mm min^{-1} and controlled ambient temperature T = 20°C in a custom-built universal testing machine (MTS, 15 kN cylinder). At least two tensile and shear tests were conducted for each type of exposure. From the two system specimens exposed to combined loading, three to four sections were available each for tensile and shear testing.

2.3 | Dynamic mechanical analysis

DMA of the prism-shaped silicone samples were conducted with an Anton Paar MCR501 device in torsional shear mode at a frequency of 1 Hz. Temperature sweeps between −85 and +100°C applied a deformation of 0.5%. This deformation lies within the linear viscoelasticity range, as amplitude sweeps at −60 and 60°C show. After cooling the samples to minimum temperature, the procedure involved a heating interval and a subsequent cooling interval, both at a rate of 1 K min^{-1}.

2.4 | Fourier-transform infrared spectroscopy

FTIR spectroscopy of the sealants was conducted with a Perkin Elmer Spectrum One device and an ATR (attenuated total reflection) sampling accessory with a diamond crystal and single reflection covering the mid-range at wave numbers between 650 and 4000 cm^{-1} at a resolution of 1 cm^{-1}. Spectra resulting from ATR-FTIR characterize the surface of the samples up to a few microns into the sealant. Here, the weathered surfaces of the sealant beads were analyzed to be able to detect possible effects of climatic and mechanical loading. The sealant surfaces of all system specimens and field samples were analyzed at two positions each. Accordingly, two scans of reference and weathered sealant and four scans with sealant after combined exposure and field exposure were made.

2.5 | Thermogravimetric analysis

For TGA, 12 to 31 mg samples from the weathered surface were heated from T = 35°C at 10 K min^{-1} in a Perkin Elmer TGA 4000. The purge gas was nitrogen to avoid partial oxidation of the silicone chain groups.[12] At T = 850°C, the purge gas was switched to oxygen while the flow rate 50 ml min^{-1} remained the same up to temperatures of 995°C. For exemplary analysis of the gas evolving during TGA of sealant *a* by transmission FTIR, the TGA 4000 and Spectrum One devices were coupled.

2.6 | Differential scanning calorimetry

The temperatures applied in the power compensation DSC device SEIKO DSC 220°C range from −165 to

+200°C and thus cover the expected glass transition temperature. A nitrogen purge of 50 ml min^{-1} maintained an inert atmosphere during scanning. Small samples were cut from each system specimen and placed in an aluminum pan. The eight samples of series A, two per system specimen, weighed between 3.9 and 6.3 mg. The four samples of series B, one per system specimen, had between 6.7 and 7.8 mg. The initial mass of field samples of sealant *a* and *b* were between 3.2 and 5.6 mg. All samples were first cooled from room temperature to −165°C. After a dwell time of 15 min, the samples were heated to 200°C and immediately cooled again to −165°C. A second heating ramp was then started after 15 min. All heating and cooling ramps operated at 10 K min^{-1}.

2.7 | Small-/wide-angle X-ray scattering

SAXS/WAXS measurements were performed on "the MOUSE instrument" (Methodology Optimization for Ultrafine Structure Exploration), a customized Xeuss 2.0 (Xenocs, France). X-rays were generated from a microfocus X-ray tube with a copper target, and a multilayer optic was employed to parallelise and monochromatise the beam to the Cu K_α wavelength of 0.1542 nm. Data collection was performed using an in-vacuum Eiger 1 M detector (Dectris, Switzerland) which was placed at multiple distances between 138 and 2507 mm from the sample. The resulting data has been processed and scaled to absolute units using the DAWN software package according to standardized procedures.[34,35] SAXS data analysis was performed using McSAS 1.3, which uses a Monte Carlo method to extract form-free size distributions.[36]

3 | RESULTS AND DISCUSSION

The mechanical characteristics of the structural bond, particularly modulus and strength, are relevant for design and approval of an SSG-joint. As previously reported,[4] the tensile and shear characteristics of sections cut from system specimens of sealant *a* and *b* are affected by the durability test program. Figure 4 illustrates the stress–strain results of the according tensile and shear tests of sections of the joint, where it was seen that the strengths and moduli, of samples exposed to combined mechanical and climatic loading, were predominantly lower than those of the non-exposed reference samples. Adapting the criterion in ETAG 002,[2] the mean tensile and shear strength of samples exposed to accelerated aging must be above 75% of the mean reference strength; sealant *a* passes, while sealant *b* fails the durability test.

Tensile and shear tests with sections from real, field-exposed SSG-joints were also conducted for sealant b (Figure S1). The initial stress–strain behavior is rather linear, resembling the behavior of the laboratory samples exposed to combined loading. However, comparability to the stress–strain results, presented in Figure 4, is limited due to diverging thickness of the laboratory and field samples that directly affects the engineering stress and strain data. Non-exposed samples of the same joint design were not available.

Material characteristics not depending on joint dimension are thus more suitable for comparative analysis. In the following, material characterizations of non-exposed, and field and laboratory exposed silicone sealants are presented and compared in an aim to detect degradation due to aging and mechanical loading.

3.1 | Dynamic mechanical analysis

The storage modulus and loss factor, shown in Figures 5 and S2, characterize the dynamic mechanical behavior of differently exposed structural sealants *a* and *b* at increasing temperature. The strongly changing storage moduli and peaks of the loss factor at temperatures of ca. −40°C are associated with melting of crystalline phases, that formed during the previous cooling interval (Figure S3). As service temperatures are usually higher than that value, the temperature range above the melting point is particularly relevant for studying performance characteristics of the sealants. In this temperature range, the logarithmic presentation, in Figure 5, reveals a clear difference between the storage moduli of the differently exposed samples. Storage moduli of samples of both sealants, which were previously exposed to combined loading, are significantly lower than those of the reference sample. This result is consistent with the moduli of the tensile and shear tests (Figure 4). The difference between the storage moduli is highest at temperatures between the melting temperature and ca. 20°C. At 20°C, as can be seen from Table 1, the storage modulus of sealant *a* exposed to combined loading is about half of the modulus of the reference, and only about a third in the case of sealant *b* samples, indicating that sealant *b* is more susceptible to the durability test, with sealant *a* being more resistant.

Above the melting transition, the loss factor tan(δ) of the samples of both sealants exposed to combined loading is lower than that of the reference sample. The loss factor corresponds to the dissipated energies of the system specimens recorded during combined loading, which decrease in the course of the durability test.[4]

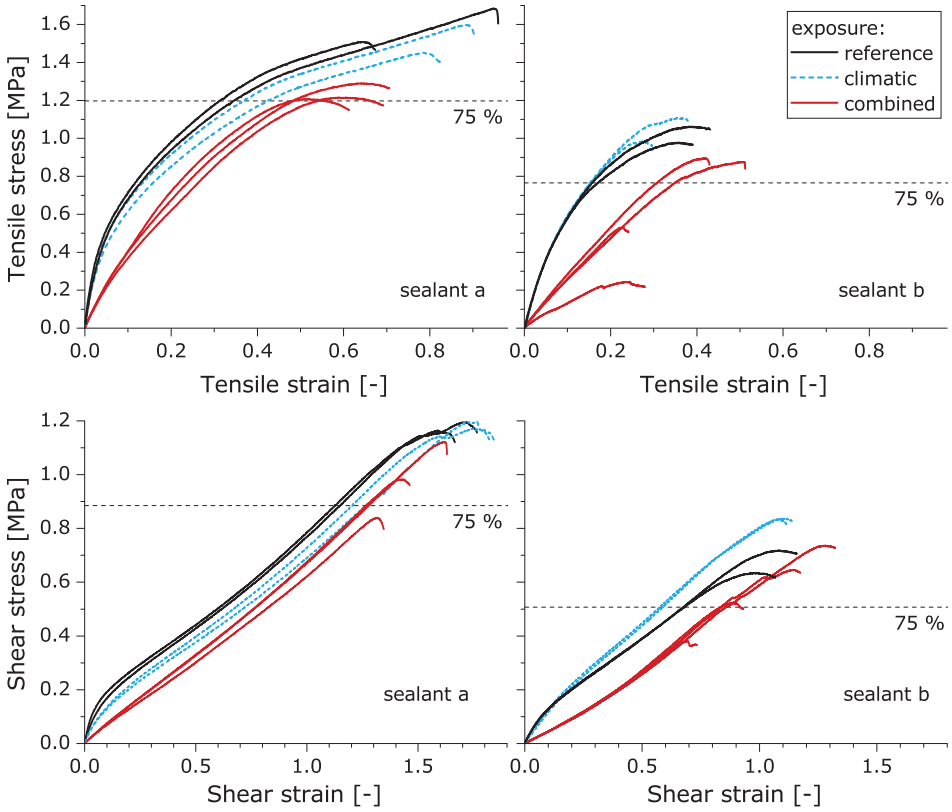

FIGURE 4 Stress–strain results from tensile and shear tests of sections cut-out from system specimens for different exposures and sealant *a* and *b*; denoted 75% of the mean reference strength give the lower strength limit for the exposed specimens [Color figure can be viewed at wileyonlinelibrary.com]

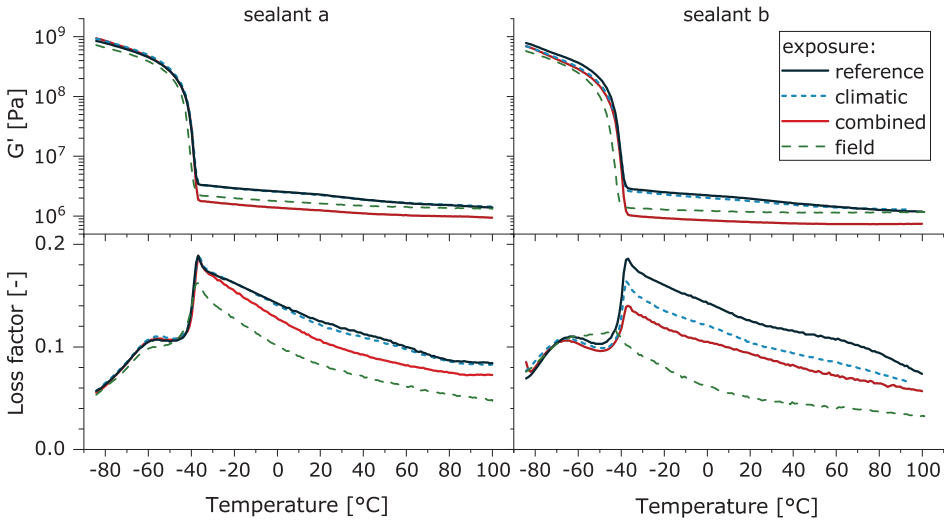

FIGURE 5 Storage moduli and loss factors of differently exposed sealant *a* (left) and *b* (right) recorded during heating [Color figure can be viewed at wileyonlinelibrary.com]

TABLE 1 Storage moduli G' at T = 20°C related to the reference value; mean values of all measurements

Exposure	Climatic	Combined	Field
Sealant a	98%	55%	77%
Sealant b	91%	38%	62%

The dynamic mechanical behavior of reference samples and of samples exposed to cyclic weathering resemble for both structural silicones, which confirms their weatherability.

Lower melting temperatures of the field samples compared to the laboratory series could result from slightly diverging silicone formulations of two batches or from different conditions during manufacturing. The storage moduli of field samples of sealant *a* and *b* are lower than those of the reference and higher than those of sealant exposed to combined loading. As expected, the durability test that was developed applying a worst case approach to simulate 50 years of exposure, is found to cause a more severe degradation of the sealants than the relatively short field exposures. Instead, loss factors of the field

samples are lower than those of the sealants exposed to combined loading. A possible explanation could be that mechanical loading of real SSG-joints occurs at higher frequencies than applied in the durability test, which may cause a stronger reduction of the damping capacity of the sealant.

3.2 | Fourier-transform infrared spectroscopy

FTIR-spectra from differently exposed samples of the two structural sealants are presented in Figure 6. Figure S4 shows the results of all analyzed samples across the full range of wave numbers. Bands of the spectra of reference, laboratory and field exposed material are similar. The spectra have silicone-characteristic peaks, that is, associated with Si—O—Si stretching at 1009 and 1080 cm^{-1}.[37] The peaks at 2963 and 2907 cm^{-1} can be assigned to symmetric and asymmetric CH_3 stretching, the peak at 1258 cm^{-1} to Si—CH_3 rocking, and the peak at 787 cm^{-1} to Si—CH_3 stretching.[37,38]

Strong peaks at 874 and 711 cm^{-1}, weak peaks at 2510 and 1795 cm^{-1}, and a broad peak between 1300 and 1500 cm^{-1} indicate the presence of a calcium carbonate filler.[28,39] As the spectra (Figure S4) do not show peaks in the range 3000–3800 cm^{-1} associated with silanol groups,[40] silica filler is not included in the formulation. If the black color of the sealants results from admixture of carbon black, the ATR-FTIR signals indicate small contents of this strongly IR-absorbing filler. High contents would affect the spectra,[41] particularly when using a diamond crystal which has a similar refractive index as carbon black.

FTIR spectra of the two types of sealant are very similar. The only notable difference lies in the peak at 1416 cm^{-1} (sealant *a*), assigned to $CaCO_3$. The corresponding peak of sealant *b* at higher bands of 1429 cm^{-1} depicts a slightly broader shape. Varied loadings and types of $CaCO_3$ could explain these differences between the spectra of the two sealants and also of field and laboratory sealants, which were manufactured from different batches of the two-component silicones. The rocking vibration of —CH2—, which is part of the crosslink between PDMS chains, absorbs IR at about 1410 cm^{-1} and between 1500 and 1600 cm^{-1}.[38,42] While a possible absorbance at the smaller wavenumber is overlaid by the broad $CaCO_3$-peak, hindering comparison, the small peaks at ca. 1580 cm^{-1} show slight differences between the two sealants with no effect coming from the types of exposure. FTIR results thus indicate no changes of crosslinking that could result from laboratory or field exposure.

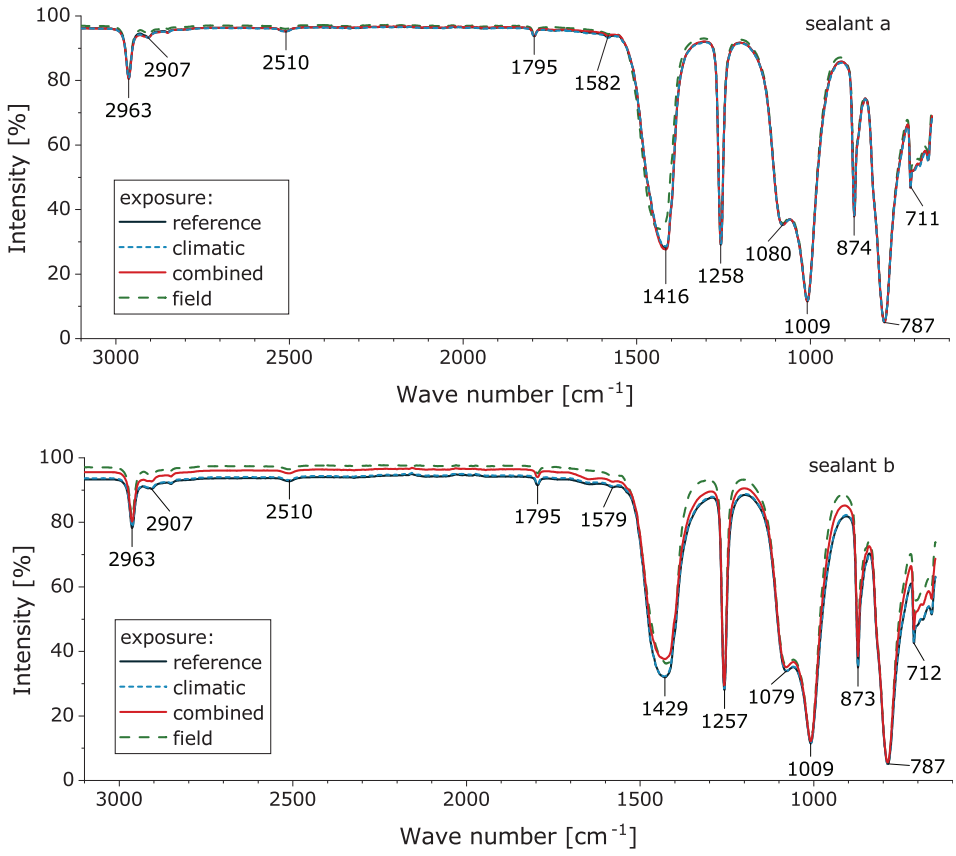

FIGURE 6 ATR-FTIR spectra of differently exposed structural sealants *a* and *b*. ATR, attenuated total reflection; FTIR, Fourier-transform infrared [Color figure can be viewed at wileyonlinelibrary.com]

3.3 | Thermogravimetric analysis

Results of TGA of differently exposed sealant *a* and *b* are shown in Figure 7, providing the relative mass and mass loss of the samples at increasing temperature. Thermal degradation of the two structural sealants occurs similarly in three phases, indicated by three local peaks of mass loss. Sealant *a* generally degrades at lower temperatures than sealant *b*. Laboratory exposure does not affect the thermal degradation of the sealants.

The results reveal some information on the composition of the sealants. Both sealants have lost only 1% of their initial mass at T = 300°C. They thus contain very small amounts of volatile components such as water and additives. The first mass loss sets in slowly at about 350–400°C, forming an asymmetric peak with maximum loss rates at about 540°C (sealant *a*) and 570°C (sealant *b*). This can be attributed to evaporation of volatile cyclic oligomers forming from PDMS chains by Si—O bond scission.[43,44] Results of TGA-FTIR analysis of sealant *a* corresponding to this 1st TGA peak, shown in Figure 8, are comparable to those seen in the literature.[45]

The overlapping second and third peak between temperatures of 650 and 800°C could be assigned to the decomposition of calcium carbonate to volatile CO_2 and remaining CaO.[28,44,46] TGA-FTIR analysis of sealant *a* confirms the presence of CO_2 in the evolved gas during the 2nd and 3rd peak, as the respective spectra in Figure 8 show CO_2-characteristic peaks at ca. 2360, 2322 cm^{-1} and 670 cm^{-1}.[47,48] Supposing that the 2nd and 3rd peaks are associated with thermal degradation of calcium carbonate, the volatile CO_2 constitutes 17.3% (sealant *a*) and 19.3% (sealant *b*) of the total mass. Together with the remaining CaO, the $CaCO_3$— filler makes 39.3% (sealant *a*) and 43.9% (sealant *b*) of the total mass.

Carbon fillers usually decompose when the purge gas contains oxygen. Here, switching the purge gas to oxygen at 850°C leads only to a small extra mass loss (<1%). The mass fraction of carbon black in the silicone rubbers is either small or other volatile molecules including carbon formed at lower temperatures, for example, during the second smaller mass loss. It is further possible, that the remaining CaO delays the mass transfer of oxygen to carbon black particles and also the transfer of carbon dioxide.

The residual mass of both sealants at T = 995°C is about 25%. It can be attributed to mostly CaO remaining from the calcium carbonate filler and possibly also to remnant SiO_2 from the silicone backbone.[44]

Thermal decomposition of field-exposed sealants (Figure S5) differs strongly from that of the corresponding type of sealants of the laboratory series. These deviations could result from differences between the batches and formulations of the two-component silicones regarding type and loading of filler, additives, mixing ratio, and so forth.

3.4 | Differential scanning calorimetry

Figure 9 shows scans of the heat flow per initial mass of the sample during the second heating ramp. The results of the two series and different exposures are similar. Bending of the curves at temperatures below −150°C is due to transient heating conditions. At temperatures of about −125°C, the curves show a slight indent, signaling a glass transition. Furthermore, scans of both sealants feature an endothermic peak corresponding to the melting transition.

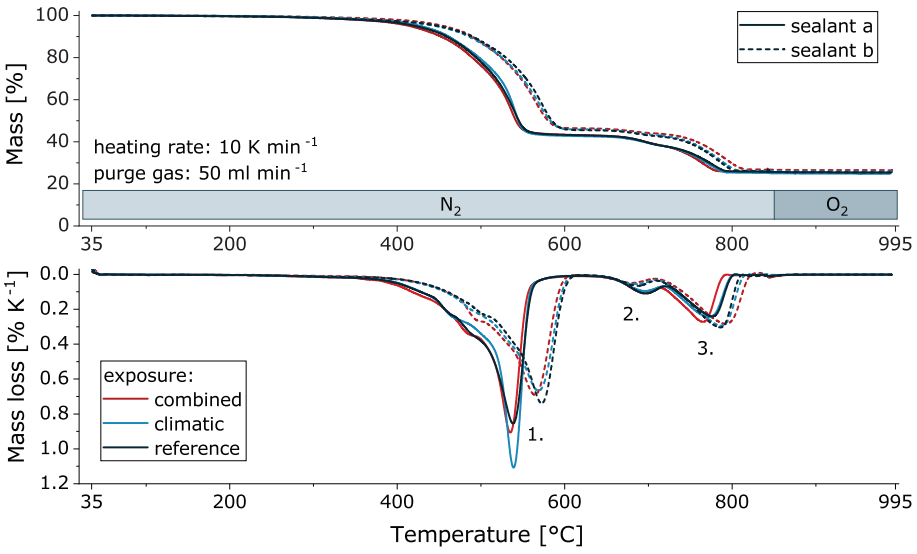

FIGURE 7 Thermogravimetric results of differently exposed structural sealants *a* and *b* [Color figure can be viewed at wileyonlinelibrary.com]

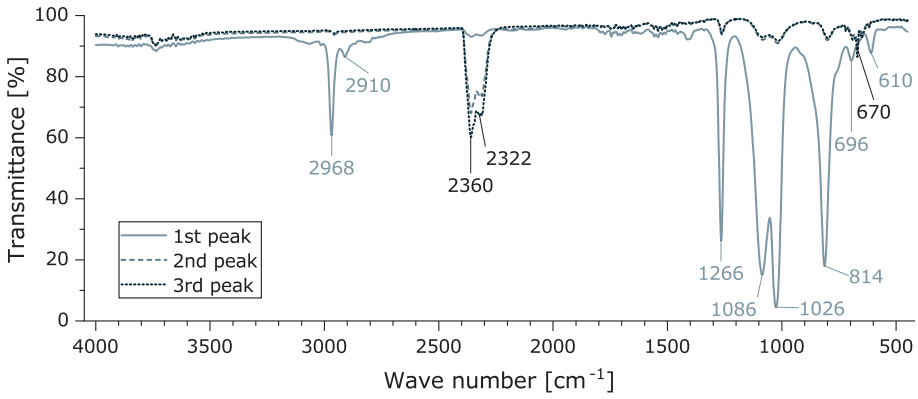

FIGURE 8 FTIR analysis of evolved gas during TGA of non-exposed structural sealant *a* corresponding to maximum mass loss of the three peaks. FTIR, Fourier-transform infrared; TGA, thermogravimetric analysis [Color figure can be viewed at wileyonlinelibrary.com]

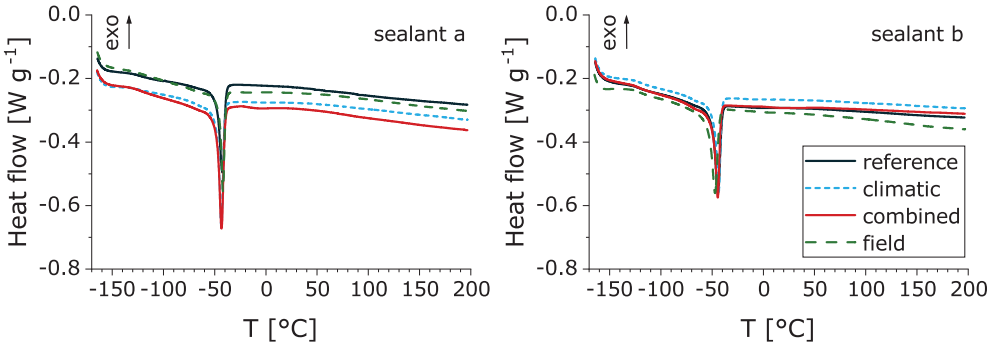

FIGURE 9 DSC results of second heating ramp of differently exposed structural sealants *a* and *b*. DSC, differential scanning calorimetry [Color figure can be viewed at wileyonlinelibrary.com]

TABLE 2 Characteristic temperatures and melting enthalpy of differently exposed structural silicone sealants *a* and *b* evaluated from calorimetric scans

Sealant	Exposure	T_g (°C)	T_m (°C)	ΔH_m (J/g)	T_c (°C)
a	Reference	$-122.3^{+0.1}_{-0.1}$	$-42.6^{+0.2}_{-0.2}$	$14.3^{+1.4}_{-1.4}$	$-73.1^{+0.8}_{-0.8}$
	Climatic	$-123.3^{+0.1}_{-0.1}$	$-43.4^{+0.3}_{-0.3}$	$16.4^{+0.3}_{-0.4}$	$-70.6^{+0.8}_{-0.8}$
	Combined	$-123.3^{+0.9}_{-1.2}$	$-42.7^{+0.6}_{-0.5}$	$16.0^{+0.6}_{-1.3}$	$-70.4^{+2.0}_{-3.5}$
	Field	$-122.1^{+0.4}_{-0.4}$	$-42.8^{+1.0}_{-1.1}$	$12.6^{+3.6}_{-3.6}$	$-71.5^{+2.0}_{-2.0}$
b	Reference	−121.9	−44.7	12.8	−75.4
	Climatic	−120.5	−43.5	12.8	−69.9
	Combined	$-120.5^{+1.2}_{-1.2}$	$-44.6^{+0.1}_{-0.2}$	$13.2^{+0.4}_{-0.4}$	$-72.9^{+2.3}_{-2.4}$
	Field	$-121.4^{+0.4}_{-0.5}$	$-49.9^{+3.3}_{-3.4}$	$11.4^{+4.7}_{-2.7}$	−75.9

Table 2 summarizes mean characteristic values evaluated from DSC results. The glass transition temperature T_g is taken at the inflection point of the heat flow curve.[49] The area under the melting peak gives the melting enthalpy ΔH_m and its minimum corresponds to the melting temperature T_m. Accordingly, the crystallization temperature T_c is evaluated at maximum heat flow during the cooling interval, that preceded the second heating ramp (Figure S6).

The characteristic temperatures of samples exposed to climatic and combined loading do not deviate significantly from those of the reference samples. They are also similar for the two types of sealant. Glass transition temperature of sealant *a* tends to be slightly lower, which could be related to different formulations of the two sealants. The slightly higher melting enthalpy of sealant *a* indicates an increased degree of crystallization and longer PDMS chains in sealant *a*. Field exposed samples show small differences between the two sealants. Neither field nor laboratory exposures have a clear effect on the results of DSC of the two sealants.

3.5 | Small-/wide-angle X-ray scattering

The scattering patterns of the reference sealants and sealants exposed to combined loading are shown on an

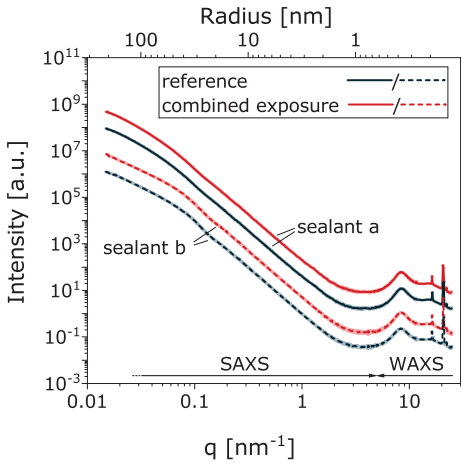

FIGURE 10 Scatter of differently exposed structural sealants *a* and *b* [Color figure can be viewed at wileyonlinelibrary.com]

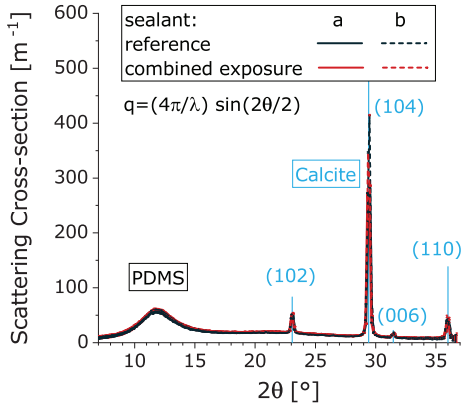

FIGURE 11 WAXS diffraction patterns in absolute scale for 2θ of differently exposed structural sealants *a* and *b*; alongside simulated calcite pattern[52] [Color figure can be viewed at wileyonlinelibrary.com]

arbitrary intensity scale in Figure 10. Segments that form the scattering patterns overlap well indicating a homogeneous distribution of filler particles for the covered q-range. Scaled SAXS/WAXS data for these samples can be found in Figure S7.

At high q, scattering of all samples is very similar. Figure 11 depicts the WAXS diffraction patterns of the four samples over the scattering angle 2θ. The observed peaks can be assigned to PDMS[50] and to calcite,[51] the $CaCO_3$-filler. The diffraction patterns show no peaks associated with carbon black filler. This may be related to the, presumably, small volume fractions of carbon black or to a type of carbon filler that has little effect on the diffraction pattern.

At low q, the scattering patterns of the two sealants *a* and *b* differ notably. Figure 12 shows the particle size distributions, extracted from the fitted scattering data associated with $q \leq 3.88\ nm^{-1}$ (Figure S8). They are essentially identical for exposed and non-exposed sealant *a*. Sealant *b* samples again show identical particle distributions, though the sample exposed to combined loading has a slightly increased total volume fraction that these particles occupy (by ca. 1%). In addition, the volume fraction of smaller particles with radii between 20 and 50 nm is higher. These small differences could be related to deviations of the mixing ratio during manufacturing. Aggregation or fragmentation of calcium carbonate filler cannot explain these differences, as the mean radii are the same.

However, potential changes of the volume distribution of agglomerates, which are larger than the covered scattering length scale, could only be studied with the implementation of ultra-small-angle X-ray scattering (USAXS).

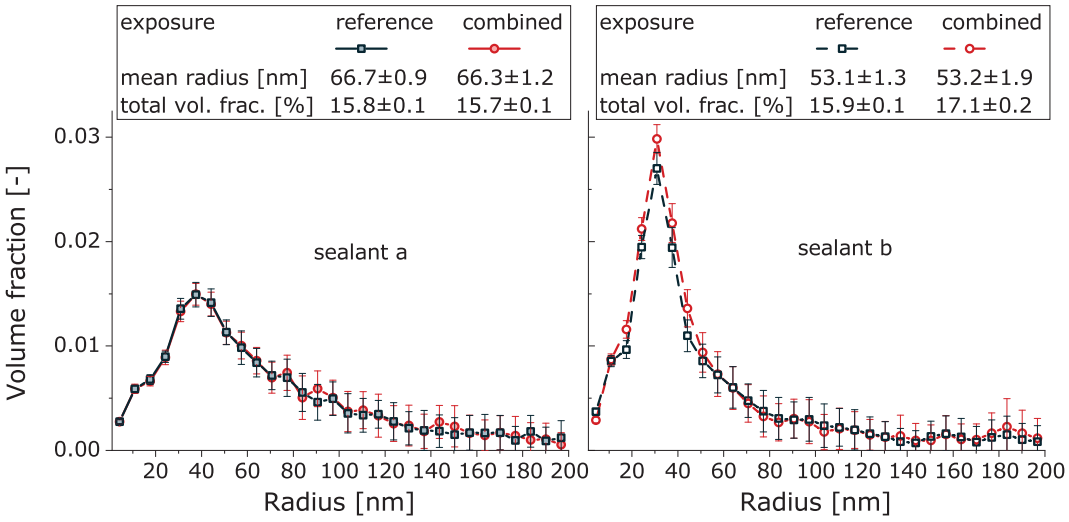

FIGURE 12 Particle size distributions of $CaCO_3$ filler in reference and laboratory exposed structural sealants *a* and *b* [Color figure can be viewed at wileyonlinelibrary.com]

4 | CONCLUSION

To approach the paramount problem of durability assessment of structural silicone joints, this paper applies selected characterization methods to identify possible effects of aging and fatigue on the silicone materials. On that account, a durability test, that simultaneously applies mechanical and climatic loads, serves as a means to induce aging and fatigue mechanisms in the silicone bonds. Sealant material from specimens of two such laboratory test series (two structural silicones) and field samples of the same type of silicone were subjected to DMA, FTIR, DSC, TGA, and SAXS/WAXS measurements.

The results show that neither laboratory nor field exposure cause notable changes of the analytical characteristics of the sealants. It can be concluded that the characterization methods deployed in this paper show no sensitivity toward combined loading of the silicone sealants. Nevertheless, results of the applied characterization methods differentiate the two studied SSG-silicones, with TGA, FTIR, and SAXS/WAXS indicating different types and loadings of $CaCO_3$ filler and DSC revealing differences between the PDMS chain lengths and formulations of the two sealants.

DMA of the sealant and shear and tensile testing of the bond so far are the most appropriate methods for performance and durability assessment of structural sealants and SSG-systems. However, the performance of the bond remains particularly relevant as it includes not only the cohesive but also the critical adhesive part of the SSG-joint.

The reduced mechanical characteristics of sealant exposed to combined loading cannot be explained with changes of the molecular structure or the morphology, such as a possible aggregation or dispersion of filler particles. Instead, they could be caused by the formation of micro-cracks and notches in the sealant bead and close to the adherends. Other characterization methods such as solvent swelling, contact angle (wettability of the surface), scanning electron microscopy (SEM), Raman spectroscopy, and USAXS could be deployed in future studies on aging and fatigue of structural silicones.

ACKNOWLEDGMENTS

Open Access funding enabled and organized by Projekt DEAL.

ORCID

Wilma Wallau https://orcid.org/0000-0002-7111-0907
Glen J. Smales https://orcid.org/0000-0002-8654-9867

REFERENCES

[1] C. White, K. Tan, A. Wolf, L. Carbary, *Advances in Structural Adhesive Bonding*. (Ed: D. Dillard) Woodhead Publishing, Boca Raton, USA **2010**, Ch. 4, p. 66.
[2] EOTA, ETAG 002 - Guideline for European Technical Approval for Structural Sealant Glazing Kit, Part 1: Supported and Unsupported Systems (**2012**).
[3] W. Wallau, C. Recknagel, *Polym. Test.* **2019**, *79*, 106030.
[4] W. Wallau, C. Recknagel, *J. Adhes.* **2020**, 1.
[5] D. Braun, H. Cherdron, M. Rehahn, H. Ritter, B. Voit, *Polymer Synthesis: Theory and Practice - Fundamentals, Methods, Experiments*, Vol. 5, Springer, Berlin, Heidelberg **2013**.
[6] T. Lee, A. Wolf, *Durability of Building Sealants - State-of-the-Art Report of RILEM TC 139-DBS*. (Ed: A. Wolf), RILEM Publications SARL, Cachan, France **1999**, Ch. 10, p. 203.
[7] R. Young, D. Al-Khudhairy, A. Thomas, *J. Mater. Sci.* **1986**, *21*, 1211
[8] G. Momen, M. Farzaneh, *Rev. Adv. Mater. Sci.* **2011**, *27*, 1.
[9] J. Klosowski, A. T. Wolf, *Sealants in Construction*, 2nd ed., CRC Press, Boca Raton **2015**.
[10] A. Wolf, K. Oba, *Durability of Building Sealants - State-of-the-Art Report of RILEM TC 139-DBS*. (Ed: A. Wolf) RILEM Publications SARL, Cachan, France **1999**, Ch. 17, p. 323.
[11] A. M. Stricher, R. G. Rinaldi, C. Barres, F. Ganachaud, L. Chazeau, *RSC Adv.* **2015**, *5*, 53713.
[12] M. Andriot, S. H. Chao, A. Colas, S. E. Cray, F. de Buyl, J. V. DeGroot, A. Dupont, T. Easton, J. L. Garaud, E. Gerlach, F. Gubbels, M. Jungk, S. Leadley, J. P. Lecomte, B. Lenoble, R. Meeks, A. Mountney, G. Shearer, S. Stassen, C. Stevens, X. Thomas, A. T. Wolf, *Inorganic Polymers*. (Eds: R. De Jaeger, M. Gleria) Nova Science Publishers, New York, USA **2007**, p. 61.
[13] A. Bele, G. Stiubianu, S. Vlad, C. Tugui, C. D. Varganici, L. Matricala, D. Ionita, D. Timpu, M. Cazacu, *RSC Adv.* **2016**, *6*, 8941.
[14] M. Frounchi, S. Dadbin, F. Panahinia, *Nucl. Instrum. Methods Phys. Res., Sect. B* **2006**, *243*, 354.
[15] O. A. Al-Hartomy, M. Ibrahim, A. Al-Ghamdi, N. Dishovsky, M. Ivanov, M. Mihaylov, F. El-Tantawy, *J. Compos. Mater.* **2012**, *46*, 1765.
[16] X. Xu, C. Gao, Q. Zheng, *Polym. Eng. Sci.* **2008**, *48*, 656.
[17] Y. Zhou, S. Wang, Y. Zhang, Y. Zhang, X. Jiang, D. Yi, *J. Appl. Polym. Sci.* **2006**, *101*, 3395.
[18] L. Yang, Y. Hu, H. Guo, L. Song, Z. Chen, W. Fan, *J. Appl. Polym. Sci.* **2006**, *102*, 2560.
[19] B. Van Lancker, J. Dispersyn, W. De Corte, J. Belis, *Eng. Struct.* **2016**, *126*, 237.
[20] Y. Sun, D. Wan, Y. Bao, X. Liu, Y. Qiu, *Key Engineering Materials*. **2018**, *768*, 13.
[21] K. Machalická, M. Vokáč, M. Eliášová, *Int. J. Adhes. Adhes.* **2018**, *83*, 168.
[22] D. Oldfield, T. Symes, *Polym. Test.* **1996**, *15*, 115.
[23] J. Y. Guan, *Durability of Building and Construction Sealants and Adhesives*. (Eds: C. White, H. Miyauchi) Vol. 6, ASTM International, West Conshohocken, PA, USA **2018**, p. 168.
[24] S. Kashi, R. Varley, M. De Souza, S. Al-Assafi, A. Di Pietro, C. De Lavigne, B. Fox, *Polym.-Plast. Technol. Eng.* **2018**, *57*, 1687.
[25] S. H. Ding, D. Z. Liu, *Constr. Build. Mater.* **2006**, *20*, 878.
[26] M. Zhang, I. Denes, Y. Xue, M. R. Buchmeiser, *Macromol. Chem. Phys.* **2016**, *217*, 1729.
[27] R. Keshavaraj, R. W. Tock, *Polym.-Plast. Technol. Eng.* **1994**, *33*, 537.
[28] R. M. Paroli, A. H. Delgado, K. C. Cole, *Can. J. Appl. Spectrosc.* **1994**, *39*, 7.

[29] S. Sugiyama, *Third International RILEM Symposium on Durability of Building and Construction Sealants*. (Ed: A. T. Wolf), RILEM proceedings SARL, Seneffe, Belgium **2000**, p. 97. https://www.rilem.net/publication/publication/15?id_papier=1489
[30] L. D. Carbary, in *Glass Performance Days*. Tampere, Finland **2007**, p. 190.
[31] G. V. Gordon, L. D. Lower, L. D. Carbary, *Durability of Building and Construction Sealants and Adhesives*. (Ed: A. T. Wolf) Vol. 3, ASTM International, West Conshohocken, PA, USA **2010**, p. 313.
[32] H. Liu, G. Cash, D. Birtwhistle, G. George, *IEEE Trans. Dielectr. Electr. Insul.* **2005**, *12*, 478.
[33] F. de Buyl, *Int. J. Adhes. Adhes.* **2001**, *21*, 411.
[34] B. R. Pauw, A. Smith, T. Snow, N. Terrill, A. F. Thünemann, *J. Appl. Crystallogr.* **2017**, *50*, 1800.
[35] J. Filik, A. Ashton, P. Chang, P. Chater, S. Day, M. Drakopoulos, M. Gerring, M. Hart, O. Magdysyuk, S. Michalik, *J. Appl. Crystallogr.* **2017**, *50*, 959.
[36] I. Breßler, B. R. Pauw, A. F. Thünemann, *J. Appl. Crystallogr.* **2015**, *48*, 962.
[37] J. E. Mark, *Physical Properties of Polymers Handbook*, 2nd ed., Springer, New York, USA **2007**.
[38] E. Shivakumar, C. Das, K. Pandey, S. Alam, G. Mathur, *Macromol. Res.* **2005**, *13*, 81.
[39] F. B. Reig, J. G. Adelantado, M. M. Moreno, *Talanta* **2002**, *58*, 811.
[40] L. Dewimille, B. Bresson, L. Bokobza, *Polymer* **2005**, *46*, 4135.
[41] P. Wilhelm, *Micron* **1996**, *27*, 341.
[42] S. Pehlivan-Davis, J. Clarke, S. Armour, *J. Appl. Polym. Sci.* **2013**, *129*, 1446.
[43] G. Camino, S. Lomakin, M. Lazzari, *Polymer* **2001**, *42*, 2395.
[44] S. Hamdani, C. Longuet, J.-M. Lopez-Cuesta, F. Ganachaud, *Polym. Degrad. Stab.* **2010**, *95*, 1911.
[45] X. Gao, H. Liu, H. Wei, J. Zheng, G. Huang, *Polym. Bull.* **2019**, *76*, 2835.
[46] A. M. S. Mandalihan, J. L. Sitjar, E. Magdaluyo Jr.., *Materials Science Forum*. **2016**, *864*, 23.
[47] C. Zhou, L. Yu, W. Luo, Y. Chen, H. Zou, M. Liang, *J. Appl. Polym. Sci.* **2015**, 41619.
[48] E. Pretsch, P. Bühlmann, M. Badertscher, *Structure Determination of Organic Compounds*, 4th ed., Springer, Berlin **2009**, p. 269.
[49] J. D. Menczel, L. Judovits, R. B. Prime, H. E. Bair, M. Reading, S. Swier, *Thermal Analysis of Polymers: Fundamentals and Applications*. (Eds: J. D. Menczel, R. B. Prime) John Wiley & Sons, Hoboken, NJ, USA **2009**, p. 7.
[50] Y. Ji, M. Zhang, K. Guan, J. Zhao, G. Liu, W. Jin, *Adv. Funct. Mater.* **2019**, *29*, 1900735.
[51] G.-T. Zhou, J. C. Yu, X.-C. Wang, L.-Z. Zhang, *New J. Chem.* **2004**, *28*, 1027.
[52] E. Maslen, V. Streltsov, N. Streltsova, *Acta Crystallogr., Sect. B: Struct. Sci.* **1993**, *49*, 636.

SUPPORTING INFORMATION

Additional supporting information may be found online in the Supporting Information section at the end of this article.

How to cite this article: Wallau W, Recknagel C, Smales GJ. Structural silicone sealants after exposure to laboratory test for durability assessment. *J Appl Polym Sci*. 2021;e50881. https://doi.org/10.1002/app.50881